Visual
Abstract

The earth-fill dam state express investigation using mechanical vibrations produced by HPP

Galina Antonovskaya

N. Laverov Federal Center for Integrated Arctic Research of the Ural Branch of the Russian Academy of Sciences, Russian Federation
essm.ras@gmail.com, http://orcid.org/0000-0002-8105-5892

Natalia Kapustian

N. Laverov Federal Center for Integrated Arctic Research of the Ural Branch of the Russian Academy of Sciences, Russian Federation
Schmidt Institute of Physics of the Earth of the Russian Academy of Sciences
nkapustian@gmail.com, http://orcid.org/0000-0002-3478-2691

ABSTRACT. The usage of mechanical vibrations produced by the hydropower plant (HPP) turbine may be used for seismic sounding of large-scale constructions as the earth-fill dam and its abutment contacts. Such vibrations are monochromatic oscillations at main frequencies and their harmonics produced by turbine. Seismic sensors installed on the dam's crest and inside it, if it possible, and in the area of abutment contacts register microseisms include HPP turbine operation vibrations which may be extracted by seismic data processing, i.e., filtering. We discuss two data processing possibilities: symphonious filter as the hardware one and power spectrum calculation as digital one. We consider the two case of earth-fill dams state investigations. There are the Chiryurt HPP dam (Republic of Dagestan, Russia, 37.5 m height) and the Nurek HPP dam (Tajikistan, 300 m height). We show the possibilities of seismic express investigations using signals of main frequencies produced by HPP turbine for dam sounding. For Chiryurt dam the extra fluid filtering in the central part of the dam was revealed. Nurek dam abutment contact monitoring showed the temporal variation of its stress-strain state associated with deformation variation 10^{-5}-10^{-6} presumably due to regional seismicity.

KEYWORDS. Hydropower plant, Turbine vibration, Seismic data processing, Filtration, Dam state monitoring, Express investigation.

OPEN ACCESS

INTRODUCTION

The simplicity of the earth-fill dam design determines their wide application due to the use of local building materials, the possibility of construction in almost any geological conditions, the acceptable accuracy of available design models. Despite the existing advantages, the largest number of accidents falls on earth-fill dams [1]. The most common causes of earth-fill dam failures are follows [2-7]:

− Cracking due to settlement (transverse cracks) or a landslide (longitudinal cracks);
− Shearing failure along a sliding surface in the dam body or in the sub-base;
− Dam overtopping due to insufficient spillway capacity;
− Failure due to a landslide in the reservoir;
− Internal erosion in the case of an uncontrollable leakage through the dam body or through its sub-base;
− Failure due to erosion by water flow or due to the effect of water waves;
− Failure due to natural disasters (earthquakes and heavy rains).

Failures due to internal erosion may occur in the case of an uncontrollable leakage through the dam body, or through its sub-base. Such failures represent approximately 40 % of all failures of earth fill dams. The loss of stability can manifest in the form of a downstream and upstream slope failure or in the form of cracks in the dam body.

As noted in Jandora and Riha [8], the above-mentioned types of failures are interrelated, and many times these failures manifest themselves at the same time or produce one another. For example, uncontrolled leakage may cause a change in the structure of the dam material and may lead to loss of stability. On the other hand, local landslides may shorten the seepage path, increase the hydraulic gradients, lead to the formation of a privileged path, and consequently result in hydraulic failure. Surface erosion may lead to loss of dam stability.

In general, dams are systematically surveyed on the basis of geodetic, geotechnical and seismic methods, for example [9-13]. Some authors use GNSS techniques [14, 15], interferometric synthetic aperture radar (InSAR) methods [16-19], spirit leveling [20, 21] and motorized control total stations systems [9, 22]. In [23] noted that to make intelligent decisions on the selection of the optimal combination of the sensors, their optimal location and density, the design must be based not only on the geometrical strength and sensitivity of the monitoring network, but also on a good understanding of the physical process which leads to deformation.

In our opinion, the applying of mechanical vibrations from operating industrial sources is another opportunity to assess the object state especially in conditions of high levels of industrial vibrations and electrical noise and built-up areas. This approach allows quickly obtain information about the object state and make an urgent decision for detailed studies or installing a monitoring system. In [11], we considered the possibility of inspecting a gravity concrete dam with signals from a pumping unit. In this article, we propose to consider an express seismic method for assessing the earth-fill dam state, based on the use of mechanical vibrations produced by a hydropower plant (HPP) turbine.

It should be noted that the idea of using mechanical vibrations, primarily from powerful sources such as hydroelectric turbines, arose in seismology in the second half of the XX century. It was shown that in microseism spectra there are thin peaks corresponding to monochromatic signals. Such peaks were ubiquitous [24-30], even at the ocean bottom [31]. Researchers were revealed their main properties such as small variations in main frequencies and their harmonics over time, correlated with variations in the frequency of the electrical network. The value of the seismic frequency in all our studies is $f = 50/N$, where N is an integer associated with the number of electric machine pairs of poles. All this pointed to the nature of the signal – the propagation in the medium of mechanical vibrations created during the operation of HPP turbines.

NORSAR seismic network made one of the first observations of the signal at main frequencies produced by the Handerfossen hydroelectric power plant in Norway and used of this signal for the Earth's crust investigation [32]. This work aroused interest, especially in the Russian Federation in connection with the research program "Vibrational sounding of the Earth" [33]. Observations of such signals were considered as reconnaissance survey to create powerful vibrators, for example [34-36]. The results justified the possibility of receiving weak signals at large (more than 100 km) distances from the source by extracting a monochromatic signal from microseisms (by filtering or accumulation). After this task was solved, scientific interest weakened. The reason is that seismic vibrators began to be used for geophysical goals of geological environment structure studying. There are special methods for the applied tasks of structures survey, and the introduction of new ones into practice requires adjustment of standards. Nevertheless, the advantages of the monochromatic mechanical signals (the constant in time operation of the source, the possibility of registration on noisy and inconvenient sites for placing vibrators, etc.) stimulated the continuation of academic research for promising use in practice.

The goal of this work is to present the possibilities of express methods of survey and monitoring of earth-fill dams of hydroelectric power plants using seismic vibrations created during the operation of an electric machine (HPP turbine).

MATERIALS AND METHODS

In article we consider two objects, first one is the monitoring of the Nurek HPP dam abutment contacts in Tajikistan and second one is the Chiryurt HPP dam survey in Republic of Dagestan, Russia.

Description of the research objects

The Nurek HPP dam is a rock and earth construction and one of the world's largest bulk dams, its height is 300 m. For our work, it was important that the Nurek HPP is the only one in Central Asia in terms of the number of pole pairs (N = 15), i.e. turbine generating unique vibrations at frequencies F = 3.(3); 6.(6); 9.(9) Hz. The seismic signal was recorded at distances from 0.5 to 120 km, and in different azimuths from the HPP [37-39]. Monitoring experiment of its abutment contacts state (Fig. 1) we carried out in the 1980s, but the primary material was not interpreted in terms of temporal changes in the rock properties in the seismically active area. This work was conducted in the pre-digital era and required the creation of a special device - a hardware synchronous filter, which accumulated the recorded seismic signal by digitizing it using a signal of the electrical network [37]. This made it possible to eliminate the "floating" of the seismic frequency, because it is associated with the "floating" of the frequency of the electrical network.
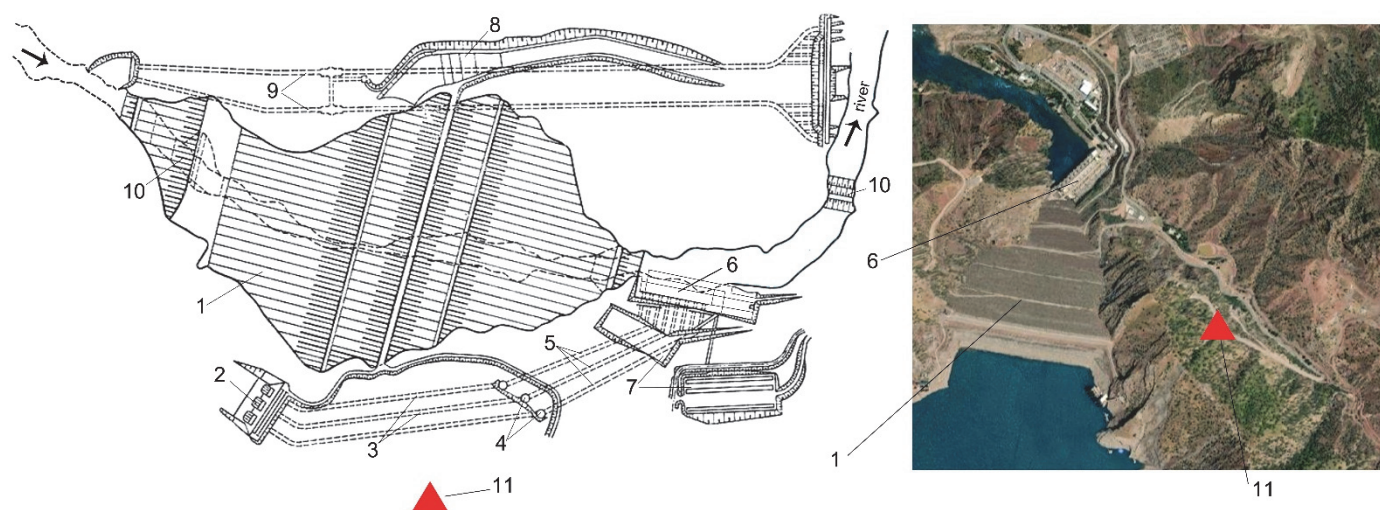
Figure 1: Scheme of the Nurek hydroelectric power station on the Vakhsh river and its view: 1 – dam; 2 – intake channel; 3 – pressure water supply tunnels; 4 – compensating reservoirs; 5 – turbine water pipelines; 6 – HPP building; 7 – open switchgear; 8 – open spillway with a tailrace canal; 9 – construction tunnels; 10 – riding and grass-roots bulkheads. 11 – location of the seismic registration station.

Registration the seismic signal produced by the Nurek HPP was carried out in the tunnel, which reduced the effect of atmosphere pressure and temperature variations. We used a vertical seismometer SM3-KV (designed and manufactured by Geophysical Survey of RAS, Russia), frequency range 0.5–50 Hz, sensitivity is 120–170 V/m/s, dynamic range is 96 dB. The extracting signal produced by HPP turbine was carried out directly by accumulation using a synchronous filter. Registration was conducted during one week with time interval 1 hour.

The Chiryurt HPP complex includes 3 power plants, they are Chiryurt HPP-1, Chiryurt HPP-2 and Gelbakh HPP, differing in the number of pole pairs, i.e., main vibration frequencies. The Chiryurt dam, common to all hydropower plants, is an earth-fill dam with a clay core; length is 430 m, maximum height is 37.5 m; the width of the ridge is 9.5 m (Fig. 2). The bottom concrete spillway in the body of the earth dam is combined with the water receiver; the spillway is 34 m long and is designed to carry 3000 m^3/s of water. Along the crest of the dam there is a highway with a heavy traffic of cars. A scheme of seismic investigations is shown in Fig. 3.

Working hydro turbines are at 4 km from the dam. We used three-axis strong-motion force feedback accelerometers CMG-5T (designed and manufactured by Güralp Systems Limited, United Kingdom) with 24-bit digitizers GSR-24 (designed and manufactured by GeoSIG Ltd, Switzerland), horizontal components are oriented along and across the dam to record signals from hydroelectric turbines. Additionally, we passed a detailed profile with seismometers SM3-KV having one vertical component (designed and manufactured by Geophysical Survey of Russia Academy of Sciences, Russia). In the absence of

the required number of seismic sensors, the work was carried out according to the following scheme. One sensor was installed stationary in the middle of the dam's crest. Other sensors (it may be one) perform sequential registration of microseisms at the *i*-th points of the dam's crest. Next, the level of microseisms at each *i*-th point calculated relative to the stationary point.
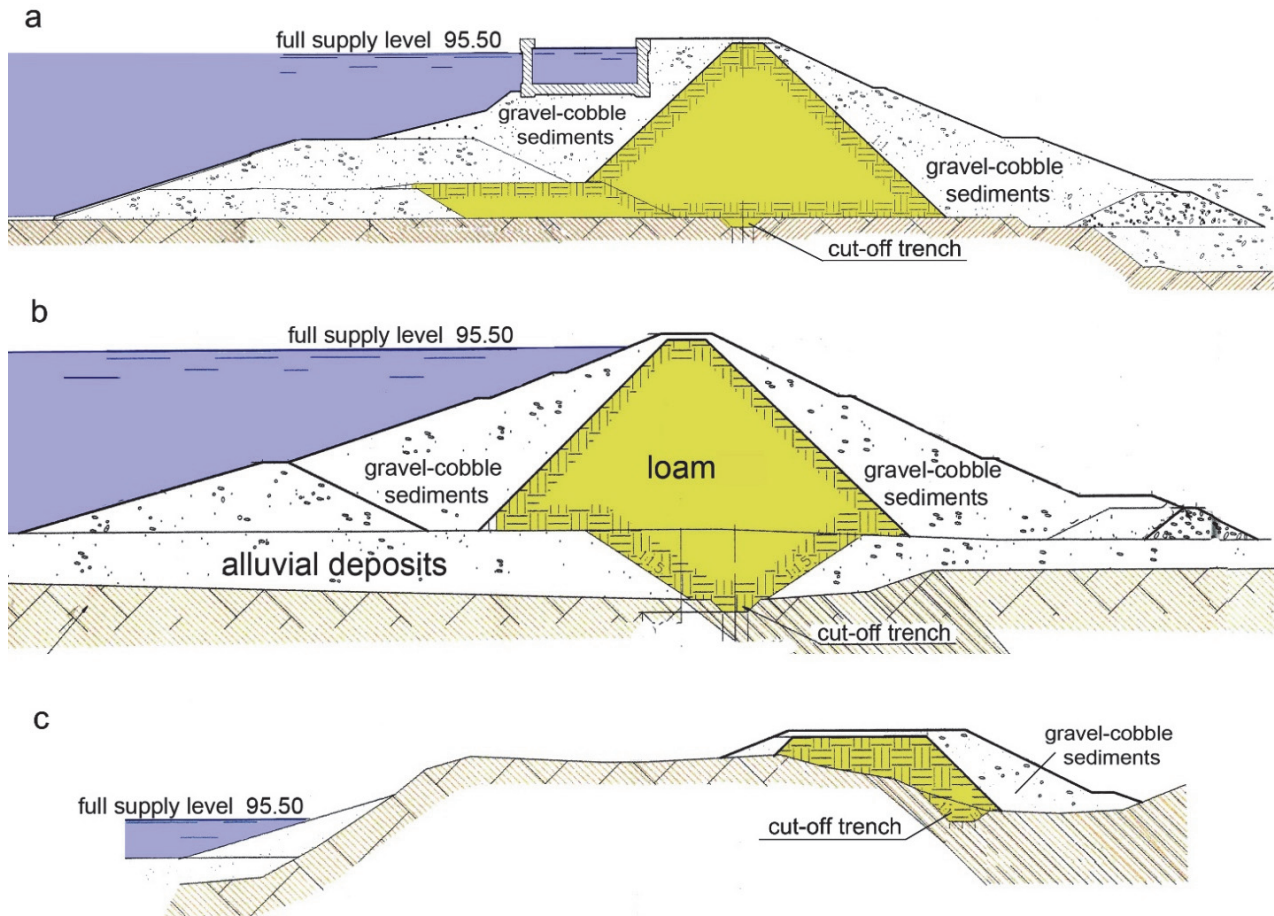
Figure 2: Cross section of the Chiryurt dam: a – left, b – middle, c – right.
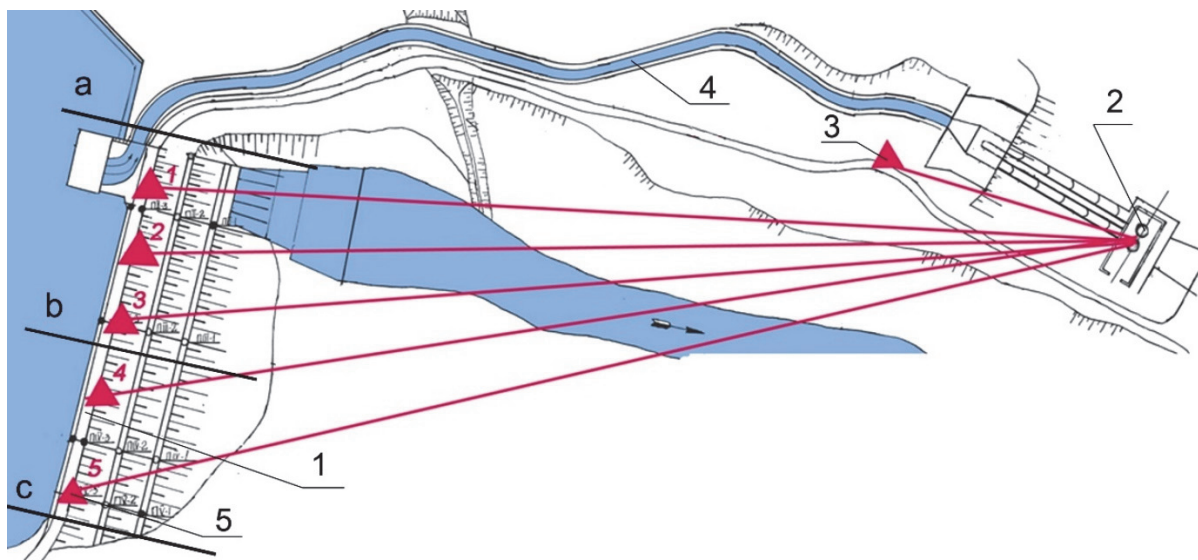
Figure 3: Scheme of the Chiryurt dam seismic sounding by mechanical vibrations produced by HPP turbine with accelerometers CMG-5T: 1 – earth-fill dam, 2 – HPP-1 building, 3 – seismic checkpoint, 4 – derivation channel, 5 – placement of seismic sensors. Cross-sections a, b and c correspond cross-sections on Fig. 2.

The duration of microseism record 20 minutes is a sufficient condition in the absence of other man-made sources, for example, passing vehicles. If there is a lot of man-made noises, then we recommend increasing the duration of microseisms registration at each point up to 60 minutes.

Data processing

The basis of interpretation is the amplitude value of mechanical signal produced by turbine HPP at given point and at a given time. To obtain amplitude values, various techniques were used, which are reduced to estimating the amplitude using filtering. The hardware option was created in the experiment at the Nurek HPP. We present a schematic diagram because currently this approach with real-time signal extraction can be implemented by software when monitoring objects.

Synchronous filter is a device for the ability to conduct express processing designed to detach sinusoidal and quasi-sinusoidal signals by accumulation. The operation principle is as follows. The input is attached to superposition of the studied signal and noise. The switch divides the continuous information into segments, the duration of which is equal to the period of the studied signal. The segments are summed up, and the power of incoherent interference increases proportionally k (the number of segments) and the power of the signal folding in the phase is k^2. The signal-to-noise ratio by power increases proportionally k. The amplitude and phase frequency characteristics of the synchronous filter are as follows:

$$R(f) = \left| \frac{\sin\left(\frac{\pi k f}{f_0}\right)}{\sin\left(\frac{\pi f}{f_0}\right)} \right| \tag{1}$$

where $\varphi(f) = exp\{i\pi(k-1)/f_0\}$; $f_0 = 1/T$ – frequency of studied signal.

Let's analyze the frequency response (Fig. 4). At frequencies that are multiples of the base frequency f_0, the signal is amplified at k times. Between the main petals, corresponding to multiples of frequencies, there are still $k-2$ parasitic petals, separated by zeros. Maxima values are reached at

$$\frac{f}{f_0} = \frac{2n+1}{2k} \tag{2}$$

zero − at

$$\frac{f}{f_0} = nk, n = 1, 2, \ldots, k-1. \tag{3}$$

The amplitude of the largest of these petals is equal to $1/\sin\left(\frac{3}{2k}\right)$ and tends to the value $0.2k$ with increasing k. The amplitude of the smallest petals tends to one with an increase k. Fig. 4a shows the set of frequency responses for $k = 2 \div 30$ of synchronous filter. It is clearly visible that with increasing k the bandwidth becomes narrower. For example, the calculation for $k = 200$ and $f_0 = 3$ Hz gives a bandwidth (at the level of 0.7) equal to 0.015 Hz.

From the formula for phase frequency response, signals at frequencies that are multiples of the base frequency either do not undergo phase distortion, or their phase changes to the reverse depending on the number of accumulation cycles. Thus, it is a filter tuned to several multiple frequencies, allowing one to amplify the signal at these frequencies and at the same time effectively suppress interference at all other frequencies.

A block-diagram of an analog synchronous filter is shown in Fig. 4. The input signal $V(t)$, which is a superposition of a microseism and a weak seismic signal, is converted $U \to F$ into a pulse repetition frequency. During one measurement cycle equal to the duration of the studied signal, the output of the converter $U \to F$ is connected alternately to the inputs of 15 counters using a switching device SD (the number 15 was chosen to study the signal from the Nurek HPP with 15 pairs of poles). Each counter measures the number of pulses, which characterizes the average value of the voltage of the

input signal $V(t)$ over time $T/15$ (T – signal period). The next switching on of the counter occurs over time T and, thus, the content of each counter characterizes the amplitude of a certain phase of the studied signal.

The tempo of synchronous switch operation is set by an external source of reference frequency, which should be 15 times higher than the frequency of the studied signal (F = $15 f_0$). Pulses of the reference frequency are fed to the input of the shift register SR, which controls the switching device. The beginning of each measurement cycle, i.e., the connection of the first counter to the input $U \rightarrow F$, is set by the pulses of the cycle start CS counter, which produces them every 15 periods of the reference frequency. Such synchronization allows you to stop the accumulation, read intermediate results and start the next portion of summation without losing the phase of the studied signal (if there is a reference frequency at the input). In addition, it is possible to work with two input signals: a second converter is used, which is connected to even counters, and the first to odd ones.
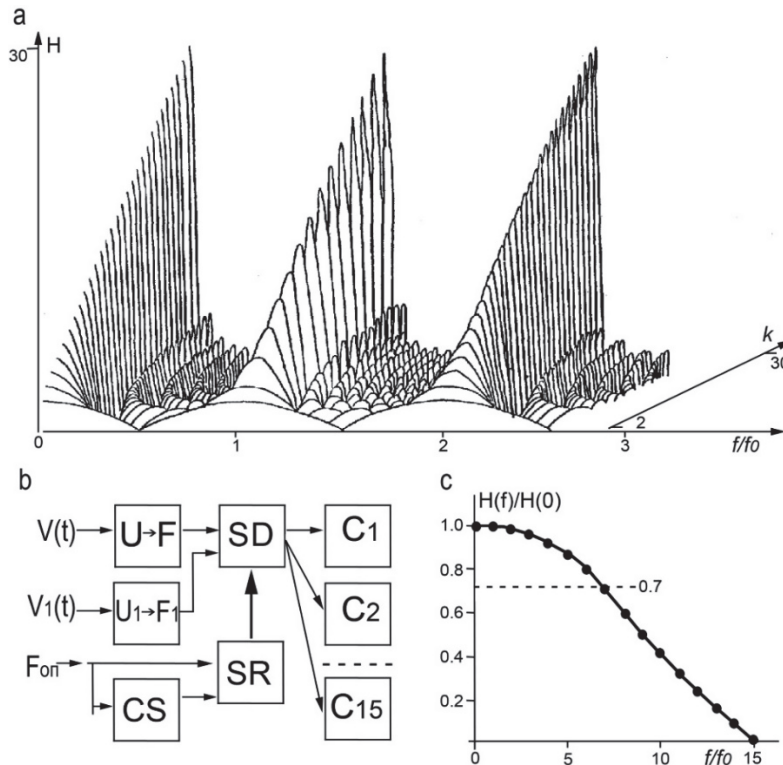
Figure 4: Synchronous filter parameters: a – frequency response (frequency response), b – block-diagram (see the description in the text), c – frequency response envelope.

It follows from the frequency response formula that the synchronous switch passes all frequencies that are multiples of the base frequency f_0. However, since each counter averages the signal over time $\left(\dfrac{1}{15}\right) f_0$, different multiples of the frequencies are skipped with different transmission coefficients. Fig. 4c shows the shape of the frequency response envelope of the synchronous switch, from which you can see that the reference frequency F is completely suppressed. At level 0.7, the synchronous filter skips the constant component and the first 7 multiple frequencies. As a reference signal, either the frequency from the generator or the electric signal (50 Hz) can be supplied. If fluctuations in the frequency of the electrical network and the seismic signal are connected (as in the case of a seismic signal from a hydroelectric power station), then the device works as a tracking filter.

In the experiments at the Chiryurt dam, we used a digital recording that allows us to extract mechanical signals produced by HPP turbine by calculating the power spectral density (PSD).

It is worth pointing out that choosing very short windows to compute PSD can lead to poor results, particularly if you have short epochs and you are interested in analyzing lower frequencies. Longer windows can result in finer resolution of PSD, but can lead to noisy PSD. One needs to strike a balance here, depending on the frequencies of interest. Highly overlapping windows does not guarantee smoother PSD estimates due to high correlation between the windows.

The amplitude of a signal along a ray distance R in a medium without intermediate boundaries is equal [40]:

$$A(R) = A(R_0) \cdot (R_0 / R)^n \cdot exp\{-\pi f_0 (R - R_0) / Q \cdot V\}, \qquad (4)$$

Where R_0 is the small distance from the source, f_0 is the frequency of the signal, the case of the predominance of absorption over scattering is considered, is the Q – quality factor of the medium, V is the propagation velocity, $n = 0.5$ for surface waves and $n = 1$ for body waves.

The signal-noise ratio (in terms of power) depends on the accumulation time and spectral density of microseisms at a given frequency in the band [41]:

$$S / N = T \cdot A^2(R) / \sigma^2. \qquad (5)$$

From (4) and (5) we get that the accumulation duration is:

$$T = M^2 \cdot \sigma^2 \cdot \left(\frac{R}{R_0}\right)^{2n} \cdot exp\left\{\frac{2\pi f_0 (R - R_0)}{Q} \cdot V\right\} / A^2(R_0) \qquad (6)$$

Let's compare the estimates obtained by the formula (4) with our data on the HPP seismic signal registration of the on the example of the Nurek HPP. In the beginning of HPP work due to technological peculiarities the main frequency was 6.6 Hz. For $f_0 = 6.6$ Hz at distance $R_0 = 2$ km and $R_1 = 15$, which are determined by our observation points location. Noise levels at registration points are comparable: $\sigma \approx \sigma_0 \approx \sigma_1$ as usual in experiments within the industrial areas. At 2 km $A(R_0) / \sigma \approx 4$, at 15 km after the accumulation of $A(R_1) / \sigma \approx 10$, i.e., at 15 km, the accuracy of determination of $M \approx 0.1$ was achieved. For body waves, assuming the ray distance $R_1 = 30$ km, $Q = 150$, $V = 4$ km/s, we get $T \approx 10^4$ c or about 3 hours of registration, which corresponds to the experiment.

RESULTS

Fig. 5 shows a typical example of waveforms registered for the Chiryurt HPP by a force feedback accelerometer installed near a working hydraulic turbine and a typical for its the microseism power spectral density. Linear peaks related to the operation of the hydraulic turbine are clearly distinguished in the PSD. The first main frequency of the hydraulic turbine operation corresponds to 3.125 Hz, the next harmonic is 6.25 Hz, then - 9.375, 12.5, 15.625 Hz, etc.
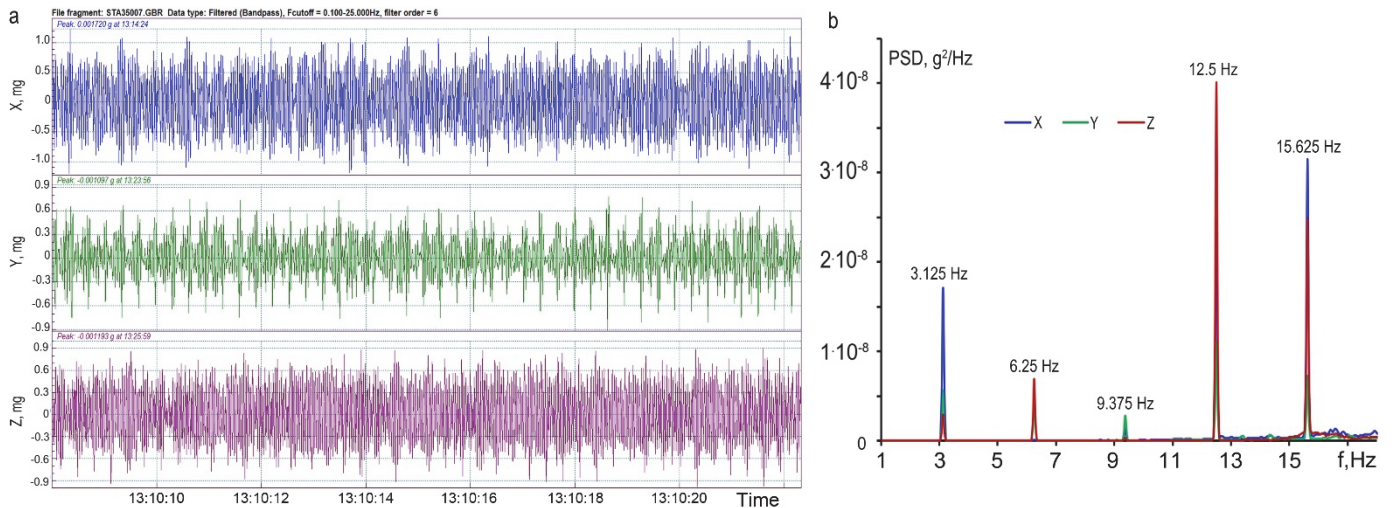
Figure 5: Typical seismic waveforms of hydraulic turbine operation in three mutually perpendicular directions (X, Y, Z) – a, and b – power spectral density for X, Y, Z components. The force-balanced accelerometer is installed next to the hydro turbine.

Fig. 6 shows the PSD for one of the registration points installed on the crest of the Chiryurt dam. The main frequency 3.125 Hz and it first harmonic 6.25 Hz are difficult to visually distinguish in the PSD due to the high level of noise from passing cars, however, these frequencies present in microseisms.

We analyzed the wave type for signal generated by the hydraulic turbine at the main and it first harmonic frequencies. For this purpose, we made a signal polarization analysis at a checkpoint located at about 0.5 km from the HPP and on the dam crest (Fig. 7). The particle trajectory shapes show that at the frequency of 3.125 Hz, the source emits a transverse wave which then adds up to the surface Rayleigh wave. For the frequency of 6.25 Hz, a mixture of longitudinal and transverse waves is already coming out of the source.
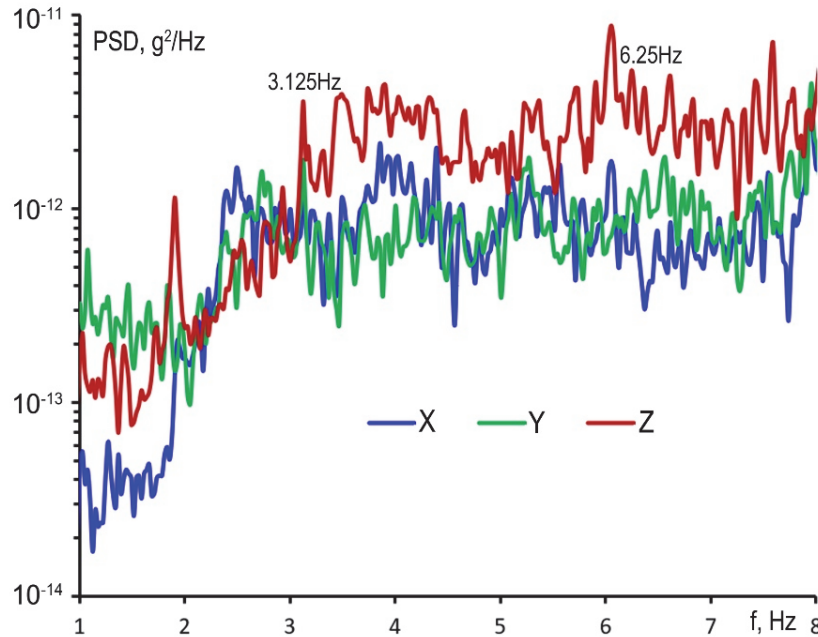
Figure 6: Typical power spectral density for X, Y, Z components for microseism registration set installed on the earthen-fill dam crest.
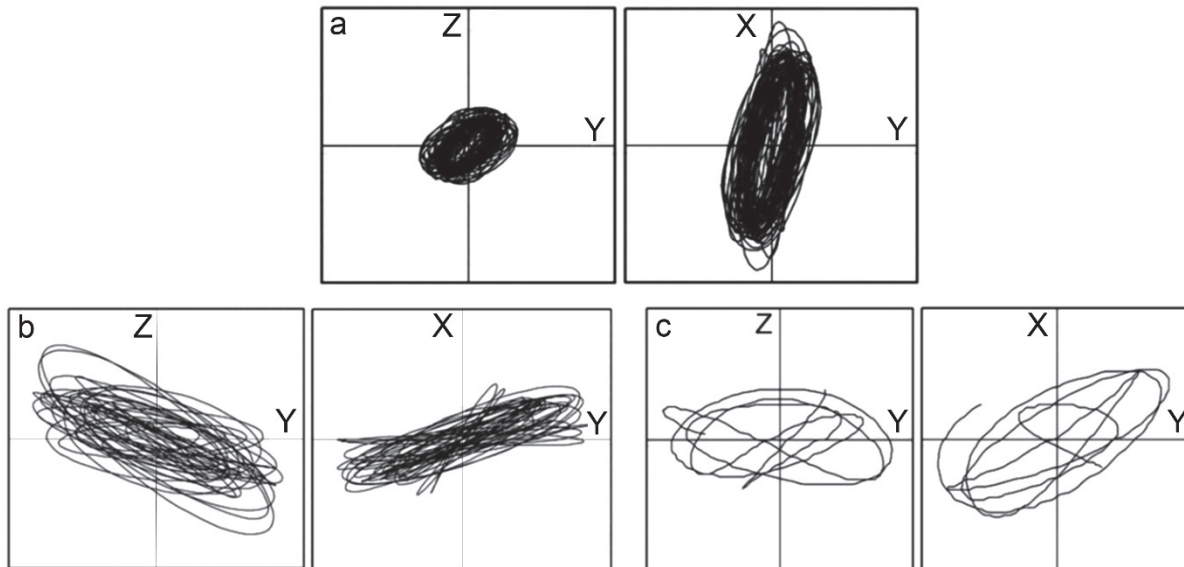
Figure 7: Particle trajectories at a distance of 0.5 km at frequencies 6.25 Hz (a) and 3.125 Hz (b) and on the dam crest at a frequency of 3.125 Hz (c).

Fig. 8 shows the signal amplitudes at frequencies of 3.125 and 6.25 Hz for the different components recorded at observation points on the dam crest. You can see that the curves for different components at 6.25 Hz are similar, and the curves for 3.125 Hz differ significantly. The curves similarity for X, Y, Z component can indicate that at the frequency of 6.25 Hz a

mixture of waves of different nature is recorded, and at the 3.125 Hz the one type of waves dominates. The results are consistent with the results of polarization analysis.

To explain the amplitude variation results, we also used additional type of impact on the dam - vibrations from cars passing along the dam crest. Subtracting from the PSD with the vehicle the background PSD gives a power spectrum density that characterizes the transport impact on the dam (Fig. 9). It should be borne in mind that the resulting PSDs contain the contribution of both the impact and the response of the structure to it.
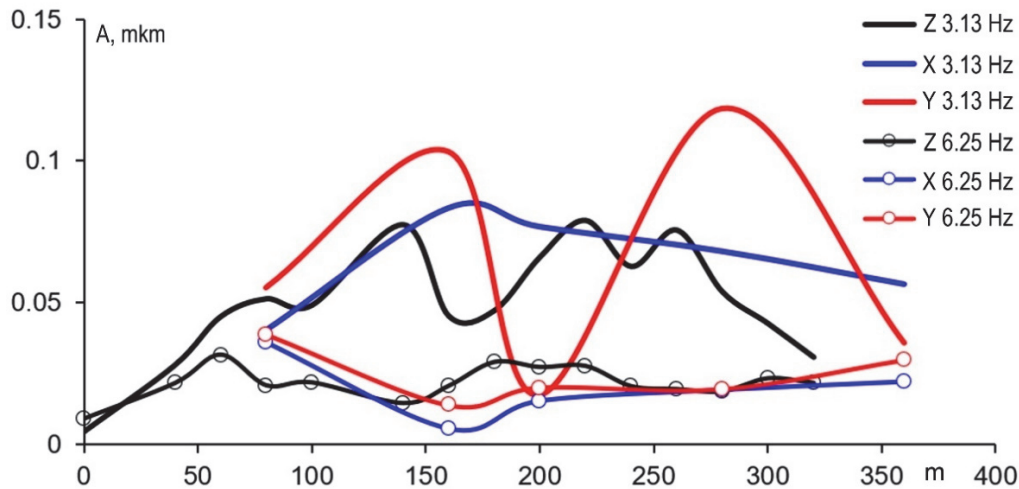
Figure 8: Distribution of amplitudes of mechanical seismic signals on the profile along the dam crest.
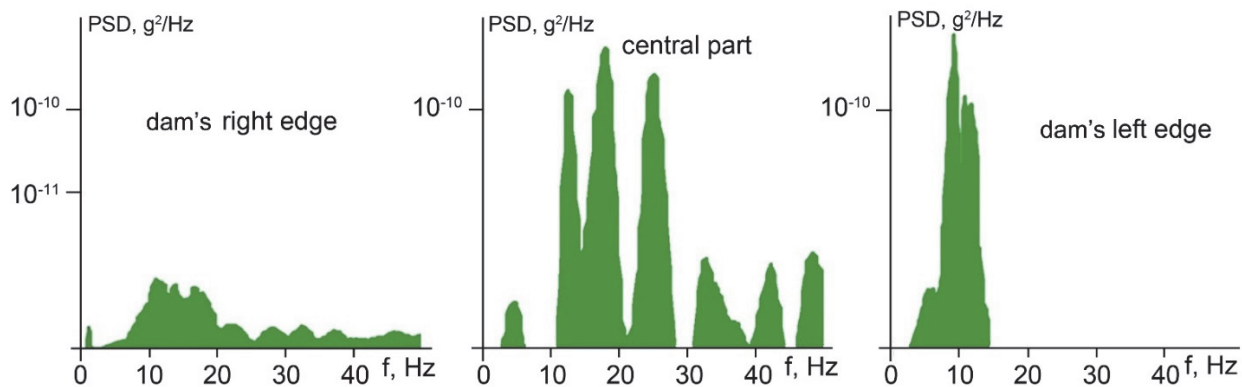
Figure 9: Typical acceleration power spectra density caused by the transport impact at the Chiryurt dam.

Let's regard of PSDs on Fig. 9, seismic sensors position and sectional view of the dam structure on its edges and in the middle (Fig 2, 3). On the right edge dam body is thin, so structure response is weaker than on the left edge and the middle part, where there are intensive PSD peaks. They may be due to the dam's core oscillation under transport impact. The highest peaks are in central part, you can see several peaks equidistant on frequency axis. This may be in the case of unfixed core moving in fluid. Such result agrees with the S-waves amplitude minimum in Fig. 8 due to water filtering. Also, the PSD levels on edges agree with amplitudes of HPP signal in Fig. 8.

The relationship of the vibration amplitude variations with the parameters of the turbine operation was analyzed during long-term observations at the Nurek HPP. Fig. 10 shows the temporal changes of the amplitudes of the main frequency 3.(3) Hz with the parameters of the HPP turbine operation. Comparison of curves shows that there is no correlation of the temporal curve of amplitudes with other curves. This suggests that variations in the amplitude of the signal that probing through the dam abutment contact are associated with a change in the stress-strain state of the rocks. The autoregression spectrum (20th order) shows the presence of daily and half- daily variations which may be due to the action of the lunisolar tide.
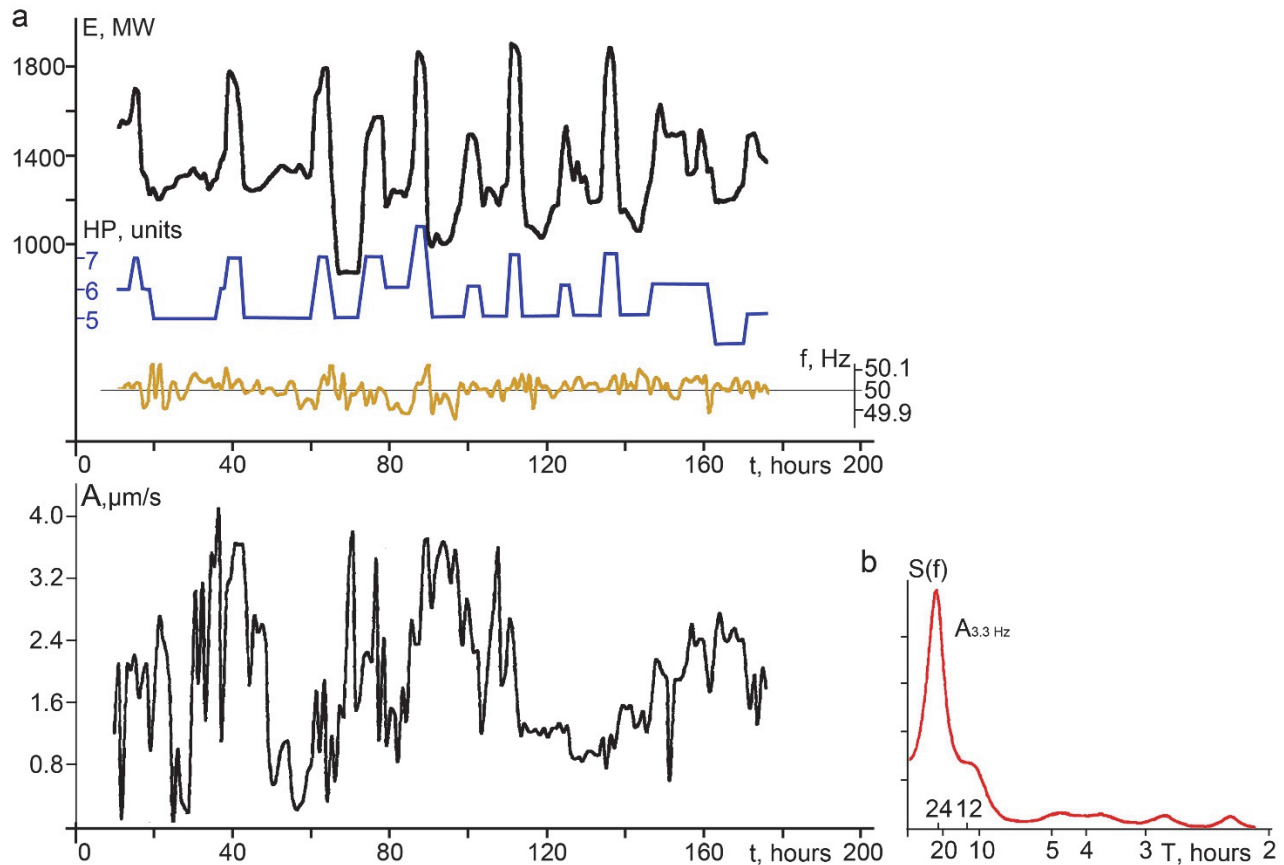
Figure 10: Time variations of the Nurek HPP turbines operation parameters and amplitudes of the main frequency of vibration at 0.5 km (a), b – autoregressive spectrum of the amplitude curve.

DISCUSSIONS

Let's analyze the results to assess the Chiryurt dam state. Since transverse waves are "sensitive" to flooding, the weakening of oscillation amplitudes in the middle of the dam indicates the presence of a moisture-saturated region. On the other hand, for the fundamental Rayleigh wave mode, the amplitude of the vertical component of the displacement velocity increases for low-velocity anomalies of the geological environment and decreases for high-velocity ones [42, 43].

Note that in Fig. 8 on the Y-component at the frequency of 3.125 Hz, predominant for transverse wave observation, there is a sharp decline at a point of 220 m (middle of the dam). At the same time, a maximum is observed on the Z component which is predominant for the Rayleigh wave. Thus, in this section of the dam, there may be both an increased water content and the presence of small voids because of suffusion. All this is possible by increasing the water filtration through the dam. Since in a signal at frequency 6.25 Hz at distances of 4 km we observe a mixture of waves, the use of it as a probing signal in this case is not effective.

A comparison of transport PSD on the right edge of the dam and in its center shows the following:

– The PSD of the dam's right edge displays mainly the vibrations created by the machine on rocky ground;
– On the vertical component, the amplification of oscillations in dam central part is visible, and additional frequencies above 10 Hz appear. These frequencies and several higher frequency maxima in the central part are located equidistantly along the frequency axis, which is typical for multiples of oscillation frequencies.

The result of sufficiently intense oscillations may indicate a relatively weak connection between the core and the base of the dam. This, in turn, corresponds to the dam sounding data by the signals from the HPP and the conclusion that increased fluid filtration is possible in the central part of the dam. In accordance with the above data, an inspection of the drainage systems of the dam was carried out with their partial restoration.

When monitoring the abutment contact of the Nurek dam, as shown above, the cause of the temporal variations in amplitudes should be sought in the change in stress-strain state of the abutment rocks.

To clarify the possible nature of the temporal variations in amplitudes, curves were divided into two components - smooth A_s (smoothing in 4 hours sliding time window) and fast ($A - A_s$). Fig. 11 compares the curves for the main frequency 3.(3) Hz in comparison with the seismicity of the Nurek district [44], Central Asia and Kazakhstan and the Northern Tien Shan for the studying time interval. A comparison of the data shows that there is no obvious connection between the moments of earthquakes and amplitude rise, but relatively large time intervals without events can be equated to sufficiently long minimums of the smooth amplitude curve.

In addition, the moments of events fall on the times when the sign of the derivative curve of the smooth component changes. In the work of [45], it was demonstrated imposition of vibration on samples leads to a change in the speed of the temporary course of plastic deformation. In the work [44] on the region seismicity analysis, it is shown that seismicity reacts not only to the absolute value of the water level in the reservoir (the value of static loading), but to a greater extent to the rate of change in the level. It is this value that is the trigger of seismicity. Thus, it makes sense to compare seismicity with the speed of deformation, i.e., with the derivative of temporal variations of smoothed amplitude.

Fig. 11 shows the temporal variations of smooth amplitudes (As), of the fast component ($A - A_s$), of the smooth amplitude derivative and the comparison of the smoothed curve the tide derivative. These temporal variations we compare with Nurek area (Fig. 11d, f) and Central Asia seismicity (Fig. 11e). You can see a rather complex connection between the events and the peculiarity of the amplitude but the sensitivity anisotropy for earthquakes from different zones of the reservoir present, solid lines for the Nurek area and dotted lines for Central Asia, help this comparison. The eastern part of the district is poorly reflected in the curve, the greatest changes are for events from the central and western parts. Unfortunately, the time series turned out to be short for obtaining bright patterns. Attention is drawn to the correspondence of the course of two curves of the derivative deformations - the smooth component and the tides, perhaps the tides play the role of a kind of "adjustment" when the geodynamics exit the equilibrium state.

The course of amplitude rapid variations is interesting, they are represented by oscillation patterns, the initial moments of which correspond to the features of the smooth component. In this regard, let us turn to the data on the initiation of unstable movement in laboratory experiments [46] in the case of movement under the influence of sinusoidally modulated voltage. Analysis of seismograms from this work for the case of impacts without movement, with a "natural" (slowly changing in time) and with initiated shifts shows that in the latter case there is an intense high-frequency wave pattern with some time delay from the load beginning.

Perhaps in our experiment there is a similar situation and the earthquakes of the area perform the impact role. Modulation of natural stress field course can be carried out by lunisolar tides, the curve of which is plotted on the graph of the fast component. In the work [46] it is noted that the shift is observed after the envelope of the sinusoidally changing load passes the maximum. Perhaps we see this situation when comparing the tide curves and the fast component when an earthquake (impact) and a tide maximum, going with the desired time delay and superimposed on the course of the smooth component, generate an oscillation pattern of the fast component. This situation is most prominently seen in an earthquake N6 and the wavetrain onset at a time of 58-60 hours.

To estimate the values of deformation changes corresponding to temporal amplitude variations, we will use the coefficient of tensosensitivity K_V for seismic wave velocities [33]:

$$K_V = (\Delta V / V) / \Delta \Theta \tag{7}$$

where $\Delta V / V$ – the relative variations in wave propagation velocity, $\Delta \Theta$ – the change in volume deformation. Experimental estimates K_V for the upper (5-10 km) part of the earth crust in a number of districts give agreed values of $10^{-3} - 10^{-4}$ with changes in velocities of 1-2% [33, 47]. The observed temporal amplitude variations during the sounding with the mechanical signal produced by HPP turbine can be estimated as $\Delta A / A \sim 100\%$. Such values correspond to $\Delta V / V \sim 1-2\%$ [38]. Taking $K_V = 10^{-3} - 10^{-4}$, we get $\Delta \Theta = 10^{-5} - 10^{-6}$ which corresponds to estimates for deformation variations in seismically active areas with the redistribution of stress fields due to tectonic processes and in the distant zone (outside the epicentral zone) of earthquakes.

The velocity amplitude (V_K) obtained by velocity-meter sensor allows us to estimate the deformations in the medium created by the passing wave [48]:

$$\varepsilon^{/} = V_K / V. \tag{8}$$

The observed value $\varepsilon^{/}$ is about 10^{-9}, i.e., sounding the medium with the help of such small deformations we obtain information about the variations in the rock deformation $10^{-5} - 10^{-6}$.
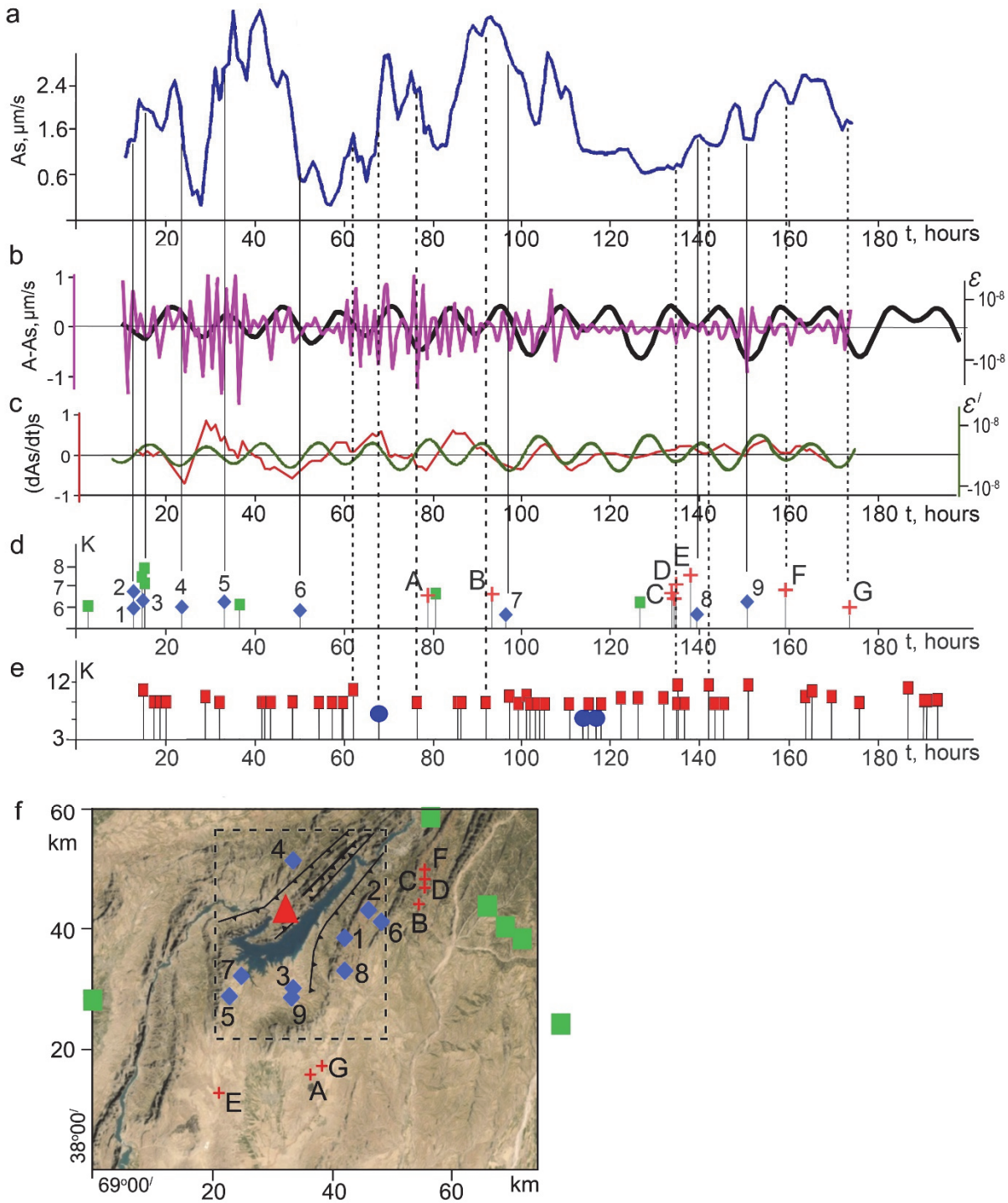
Figure 11: Seismic monitoring of the stone-earth dam abutment contacts of the Nurek HPP using mechanical vibrations produced by HPP turbine: temporal variations in amplitudes: a – smooth (As), b – fast component of the main frequency 3.(3) Hz ($A - A_s$); c – time derivatives of amplitude (dAs/dt)s and tidal deformation dε/dt; d – seismicity of Nurek district; e – seismicity of Central Asia; f – map of the epicenters of events of Nurek district, the dotted square shows the Nurek reservoir area. Icons, numbers and letters

correspond to events on (d). Letters and numbers correspond to earthquakes energy class and position. Lines: solid for Nurek area, dotted for Central Asia.

CONCLUSIONS

The considered two cases show that sounding of the earthen dam and the its abutment contacts by mechanical vibrations generated during the operation of the hydroelectric power station carries information both about the object state and about the temporal variations of the stress-strain state of the area of its location. Essentially, the sounding signal is present regardless of the experiment, i.e., we do not introduce any additional distortions into geodynamic system.

It is also important that the observations are extremely simple and the result on the dam state can be obtained quickly enough, i.e., this is an express diagnostic method. A seismometer and a recording device operating in automatic mode can be placed at almost any point, and be maintained for as long as you want (while the hydroelectric power station is operating). Thus, we consider this experiment as a model of a possible system for monitoring the environment stress-strain state in situ.

Man-made signals generated by hydraulic turbines of HPP are a good tool for detecting the process of fluid filtration into dam body.

Undoubtedly, the obtained result requires more detailed confirmation and comparison with the dam fluid filtration monitoring data. Nevertheless, the presented opportunity may be a way to improve the system for dam state monitoring, considering the economy and manufacturability of the method.

FUNDING

COMPETING INTERESTS

The authors declare that they have no known competing financial interests or personal relationships that could have appeared to influence the work reported in this paper.

REFERENCES

[1] Zhang, L., Xu, Y. and Jia, J.S. (2009). Analysis of earth dam failures: a database approach, Georisk Assessment and Management of Risk for Engineered Systems and Geohazards, 3(3), pp. 184–189. DOI: 10.1080/17499510902831759.

[2] Babu, G.L.S. and Srivastava, A. (2010). Reliability analysis of earth dams, J. Geotech. Geoenviron. Eng., 136 (7). DOI: 10.1061/(ASCE)GT.1943-5606.0000313.

[3] Foster, M., Robin Fell, R. and Spannagle, M. (2000). The statistics of embankment dam failures and accidents, Can. Geotech. J., 37 (5), pp. 1000–1024. DOI: 10.1139/t00-030.

[4] Danka, J. and Zhang, L.M. (2015). Dike failure mechanisms and breaching parameters, J. Geotech. Geoenviron. Eng., 141 (9), pp. 1957–1970. DOI: 10.1061/(ASCE)GT.1943-5606.0001335.

[5] Institution of Civil Engineers (2015). Floods and reservoir safety, ICE Publishing; 4th edition. DOI: 10.1680/frs.60067.

[6] Rodriguez, C.J.T., Needham, J.T., Torres, M.A. and Bueno, E.I. (2017). A combined risk analysis approach for complex dam-levee systems, Struct. Infrastruct. Eng., 13 (12), pp. 1624–1638. DOI: 10.1080/15732479.2017.1314514.

[7] Sanmartin, F.J., Garcia, A.L., Torres, M.A. and Bueno, E.I. (2019). Empirical tool for the assessment of annual overtopping probabilities of dams, J. Water Resour. Plann. Manage., 145 (1). DOI: 10.1061/(ASCE)WR.1943-5452.0001017.

[8] Jandora, J. and Riha, J. (2008). The failure of embankment dams due to overtopping. 169
https://www.researchgate.net/publication/40395679_The_failure_of_embankment_dams_due_to_overtopping.

[9] Acosta, L.E., de Lacy, M.C., Ramos, M.I., Cano, J.P., Herrera, A.M., Avilés, M. and Gil, A.J. (2018). Displacements Study of an Earth Fill Dam Based on High Precision Geodetic Monitoring and Numerical Modeling, Sensors (Basel, Switzerland), 18(5), 1369. DOI: 10.3390/s18051369.

[10] Akhmetov, Y.M., Assemov, K.M. and Shaytorov, V.N. (2020). Geophysical survey of earthen dam usingthe electrical prospecting methods, Contributions to Geophysics and Geodesy, 50(2), pp. 249–259.
DOI: 10.31577/congeo.2020.50.2.4.

[11] Antonovskaya, G., Kapustian, N., Basakina, I., Afonin, N. and Moshkunov, K. (2019). Hydropower dam state and its foundation soil survey using industrial seismic oscillations, Geosciences, 9 (4), 187. DOI: 10.3390/geosciences9040187.

[12] Park, D.S. and Kishida, T. (2019). Seismic response of embankment dams based on recorded strong-motion data in Japan, Earthquake Spectra, 35(2), pp. 955–976. DOI: 10.1193/042918EQS107M.

[13] Zumr, D., David, V., Krása, J. and Nedvěd, J. (2018). Geophysical evaluation of the inner structure of a historical earth-filled dam, Proceedings, 2, 664. DOI: 10.3390/proceedings2110664.

[14] Barzaghi, R., Pinto, L. and Monaci, R. (2012). The monitoring of gravity dams: two tests in Sardinia, Italy. In Proceedings of the FIGWorkingWeek (Session TS01F), pp. 1–16.
https://www.fig.net/resources/proceedings/fig_proceedings/fig2012/papers/ts01f/TS01F_barzaghi_pinto_et_al_6130.pdf.

[15] Yi, T.H.; Li, H.N.; Gu, M. (2012). Recent research and applications of GPS-based monitoring technology for high-rise structures, Struct. Control Health Monit., 20, pp. 649–670. DOI: 10.1002/stc.1501.

[16] DiMartire, D., Iglesias, R., Monells, D., Centolanza, G., Sica, S., Ramondini, M. and Calcaterra, D. (2014). Comparison between differential SAR interferometry and ground measurements data in the displacement monitoring of the earth-dam of Conza della Campania (Italy), Remote Sens. Environ, 148, pp. 58–69. DOI: 10.1016/j.rse.2014.03.014.

[17] Grenerczy, G. and Wegmüller, U. (2011). Persistent scatterer interferometry analysis of the embankment failure of a red mud reservoir using ENVISAT ASAR data, Nat. Hazards, 59, pp. 1047–1053. DOI: 10.1007/s11069-011-9816-6.

[18] Mazzanti, P., Perissin, D. and Rocca, A. (2015). Structural health monitoring of dams by advanced satellite SAR interferometry: investigation of past processes and future monitoring perspectives. 7th Internation Conference on Structural Health Monitoring of Intelligent Infrastructure.

[19] Milillo, P., Perissind, D., Salzere, J.T., Lundgrenc, P., Lacavaa, G., Milillof, G. and Serio, C. (2016). Monitoring dam structural health from space: insights from novel InSAR techniques and multi-parametric modeling applied to the Pertusillo dam Basilicata, Italy, Int. J. Appl. Earth Obs. Geoinf., 52, pp. 221–229.
DOI: 10.1016/j.jag.2016.06.013 0303-2434.

[20] Pytharouli, S., Kontogianni, V., Psimoulis, P., Nickitopoulou, A., Stiros, S., Skourtis, C., Stremmenos, F., and Kountouris, A. (2007). Geodetic monitoring of earthfill and concrete dams in Greece, Proceeding of Hydro 2006, maximizing the benefits of Hydropower,
https://www.researchgate.net/publication/292088202_Geodetic_monitoring_of_earthfill_and_concrete_dams_in_Greece.

[21] Pytharouli, S.I. and Stiros, S.C. (2009). Investigation of the parameters controlling the crest settlement of a major earthfill dam based on the threshold correlation analysis, J. Appl. Geod., 3, pp. 55–62. DOI:10.1515/JAG.2009.006.

[22] Casaca, J., Braz, N. and Conde, V. (2014). Combined adjustment of angle and distance measurements in a dam monitoring network, Surv. Rev., 47, pp. 181–184. DOI: 10.1179/1752270614Y.0000000106.

[23] Szostak-Chrzanowski, A., Chrzanowski, A., Deng, N. and Bazanowski, M. (2008). Design and analysis of a multi-sensor deformation detection system, J. of Applied Geodesy, 2, pp. 205–211. DOI: 10.1515/JAG.2008.023.

[24] Amick, H. and Gendreau, M. (2000). Construction vibrations and their impact on vibration-sensitive facilities. Construction Congress VI: Building Together for a Better Tomorrow in an Increasingly Complex World. Edited by K.D. Walsh. DOI: 10.1061/40475(278)80.

[25] Bai, L., Zhou, L., Jiang, X., Pang, Q. and Ye, D. (2019). Vibration in a multistage centrifugal pump under varied Conditions, shock and vibration, 2019, pp. 1–9. DOI: 10.1155/2019/2057031.

[26] Brezovec, M., Kuzle, I., Krpan, M. and Holjevac, N. (2020). Analysis and treatment of power oscillationsin hydropower plant Dubrava, IET Renewable Power Gener., 14(1), pp. 80–89. DOI: 10.1049/iet-rpg.2019.0523.

[27] Gieras, J.F., Wang, C. and Lai, J.C. (2006). Noise of Polyphase Electric Motors (1st ed.). CRC Press.
DOI: 10.1201/9781420027730.

[28] Limberger, F., Lindenfeld, M., Deckert, H. and Rümpker, G. (2021). Seismic radiation from wind turbines: observations and analytical modeling of frequency-dependent amplitude decays, Solid Earth, 12(8), pp.1851–1864.

DOI:10.5194/se-12-1851-2021.

[29] Svinkin, M.R. (2008). Soil and Structure Vibrations from Construction and Industrial Sources. 6th Conference of the International Conference on Case Histories in Geotechnical Engineering. https://scholarsmine.mst.edu/icchge/6icchge/session13/8/.

[30] Zakupin, A.S., Bogomolov, L.M., Mubassarova, V.A. and Il'ichev, P.V. (2014). Seismoacoustic responses to high-power electric pulses from well logging data at the Bishkek geodynamical test area, Izvestiya, Physics of the Solid Earth, 50(5), pp. 692–706. DOI: 10.1134/S1069351314040193.

[31] Bradner, H. and Dodds, J.G. (1964). Comparative seismic noise in the ocean bottom and on land, Jour. Geoph. Res., 69(20), pp. 4339–4348.

[32] Bungum, H., Risbo, T. and Hjortenberg, E. (1977). Precise continuous monitoring of seismic velocity variations and their possible connection to solid Earth tides, J. of Geoph. Research, 82 (33), pp. 5365–5373. DOI: 10.1029/JB082i033p05365.

[33] Nikolaev, A.V. (1987). Problems of nonlinear seismics. In Problems of nonlinear seismics, Moscow, Russia, pp. 5–20.

[34] Alekseev, A., Chichinin, I. and Korneev, V. (2005). Powerful Low-Frequency Vibrators for Active Seismology, Bulletin of the Seismological Society of America, 95, pp. 1–17. DOI: 10.1785/0120030261.

[35] Alekseev, A.S., Glinsky, B.M., Kovalevsky, V.V. and Khairetdinov, M.S. (2017). Geotechnologies of vibrational sounding in XXI century. Available at: https://icmmg.nsc.ru/sites/default/files/pubs/alekseev_hayretdinov_geotehnologii_vibracionnogo_zondirovaniya.pdf.

[36] Li, G., Qi, W., Ding, Y.-P., Huang, Z.-Q., Lian, Z.-H., Tao, Z.-F., and Yang, X.-Y. (2019). Method and application of extending seismic vibrator bandwidth toward low frequency, Advances in Mechanical Engineering, 11(10), 168781401988477. DOI: 10.1177/1687814019884772.

[37] Alexandrov, A.L., Volodin, A.A., Zelikman, E.I. and Nevsky, M.V. (1980). A device for studying periodic seismic signals, Seismic Instruments, 13, pp. 158–164.

[38] Kapustian, N.K. and Yudakhin, F.N. (2007). Seismic studies of technogenic impacts on the Earth's crust and their consequences. Yekaterinburg, Russia.

[39] Troitsky, P.A. (1980). Quasi-harmonic signal from the Nurek HPP at the Garmsky landfill, Izv. of the USSR Academy of Sciences. Physics of the Earth, 9, pp. 118–128.

[40] Sheriff, R.E. and Geldart, L.P. (1995). Exploration Seismology (second ed.), Cambridge University Express.

[41] Jenkins, G.M. and Watts D.G. (1968). Spectral analysis and its applications, San Francisco, Cambridge, London, Amsterdam, Holden-Day, 525.

[42] Danilov, K.B. (2017). The structure of the Onega downthrown block and adjacent geological objects according to the microseismic sounding method, Pure and Applied Geoph., 174(7), pp. 2663–2676. DOI: 10.1007/s00024-017-1542-x.

[43] Gorbatikov, A.V., Stepanova, M.Y. and Korablev, G.E. (2008). Microseismic field affected by local geological heterogeneities and microseismic sounding of the medium, Izvestiya Phys. Solid Earth, 44(7), pp. 577–592. DOI: 10.1134/S1069351308070082.

[44] Spall, H. and Simpson, D.W. (1981). The Soviet-American exchange in earthquake prediction, New York, Palisades. https://pubs.usgs.gov/of/1981/1150/report.pdf.

[45] Mirzoev, K.M., Vinogradov, S.D., Ruzibaev, Z. (1991). The influence of microseisms and vibrations on acoustic emission, Izv. of the USSR Academy of Sciences, Physics of the Earth, 12, pp. 69–72.

[46] Sobolev, G.A., Shpetzler, H. and Koltsov, A.V. (1994). Initiation of unstable motion in laboratory experiments. In Induced seismicity, pp. 62–72.

[47] Nevsky, M.V., Morozova, L.A., Starchenko, A.I. and Bezgodkov, V.A. (1987) Dependence of temporal variations of seismic wave velocities on deformation variations due to geodynamic processes. In Problems of nonlinear seismics, Moscow, Russia, pp. 203–214.

[48] Shalev, E., Kurzon, I., Doan, M.-L. and Lyakhovsky, V. (2016). Water-level oscillations caused by volumetric and deviatoric dynamic strains, Geoph. J. Intern., 204(2), pp. 841–851. DOI: 10.1093/gji/ggv483.